Journal of CO2 Utilization 60 (2022) 101978

Contents lists available at ScienceDirect

Journal of CO2 Utilization

journal homepage: www.elsevier.com/locate/jcou

Novel artificial ionic cofactors for efficient electro-enzymatic conversion of CO_2 to formic acid

Zhibo Zhang [a], Tudor Vasiliu [b], Fangfang Li [a], Aatto Laaksonen [a,b,c,d], Xiangping Zhang [e], Francesca Mocci [f,*], Xiaoyan Ji [a,*]

[a] Energy Engineering, Division of Energy Science, Luleå University of Technology, 97187 Luleå, Sweden
[b] Centre of Advanced Research in Bionanoconjugates and Biopolymers, Romanian Academy Petru Poni (PP) Institute of Macromolecular Chemistry, 00487 Iasi, Romania
[c] Department of Materials and Environmental Chemistry, Arrhenius Laboratory, Stockholm University, SE-106 91 Stockholm, Sweden
[d] State Key Laboratory of Materials-Oriented and Chemical Engineering, Nanjing Tech University, Nanjing 210009, PR China
[e] Beijing Key Laboratory of Ionic Liquids Clean Process, CAS Key Laboratory of Green Process and Engineering, State Key Laboratory of Multiphase Complex Systems, Institute of Process Engineering, Chinese Academy of Sciences, Beijing 100190, PR China
[f] Dipartimento di Scienze Chimiche e Geologiche, Università degli Studi di Cagliari, 09042 Cagliari, Italy

ARTICLE INFO

Keywords:
CO_2 conversion
Formic acid
Enzyme
Artificial cofactors
Electrocatalysis

ABSTRACT

The low yield of enzymatic conversion of CO_2 to formic acid as well as the high cost and instability of using the natural cofactor (NADH) hamper the large-scale application of the CO_2 enzymatic utilization. To address these issues and to improve the production of formic acid, six bipyridinium-based artificial cofactors were developed for the enzymatic conversion of CO_2 and further integrated with the electrocatalytic regeneration of the cofactors for the formic acid production. All of them did show a higher catalytic performance compared to NADH. Particularly, 1,1′-bis(2-(dimethylamino)ethyl)-4,4′-bipyridinium bromine did exhibit the highest catalytic performance with a high formic acid concentration of 4.76 mM in 60 min, which is 47 times higher than that of the natural cofactor NADH and is also currently the highest performance among the reported artificial cofactors in literature. Thermodynamic analysis, electrochemical investigations, and molecular dynamics simulations were performed to clarify the structure-energy relationship of the functional bipyridinium-based salts and to rationalize how it is affected by the different functional groups. This study gives a deep insight into the role of artificial cofactors in enzymatic reactions and can clearly promote the development of novel bioelectrochemical conversion of CO_2.

1. Introduction

The reduction of CO_2 and conversion into high-value chemicals and fuels is an attractive strategy for alleviating global warming and the energy crisis [1]. Among the products from CO_2 reduction, formic acid has been recognized as one of the most valuable reduction products, as it is an important chemical feedstock and hydrogen storage chemical in industries [2]. However, conventional methods for formic acid production, such as chemical-catalysis, photocatalysis, electrocatalysis, and enzymatic-catalysis, all have various drawbacks. The chemical conversion is generally conducted under harsh conditions (high pressure and high temperature), where noble metal-based catalysts are needed [3]. The photocatalysis system typically contains an electron donor, a mediator, a photosensitizer and a feedstock, being altogether a complex and unstable system, subject to difficulties in product separation due to the uncontrolled temperature caused by the light irradiation [4]. Even though electrocatalysis can achieve CO_2 conversion at a low cost (only electron is consumed), it normally suffers from a low selectivity with a diversity of products and unstable electrocatalysts even though the issue of electrocatalyst stability has been addressed a lot [5], leading to a complicated product separation and short lifetime of catalysts [6]. Enzymatic catalysis is a promising method and able to achieve a high selectivity in formic acid production under mild conditions but limited by the high cost, especially when using the natural cofactor NADH [7]. Therefore, more research is needed for formic acid production to overcome the drawbacks encountered in the conventional methods.

Recently, enzymatic electrosynthesis, i.e., an integration of enzymatic catalysis and electrocatalysis, has received much attention in

* Corresponding authors.
E-mail addresses: fmocci@unica.it (F. Mocci), xiaoyan.ji@ltu.se (X. Ji).

https://doi.org/10.1016/j.jcou.2022.101978
Received 14 January 2022; Received in revised form 11 March 2022; Accepted 13 March 2022
Available online 19 March 2022

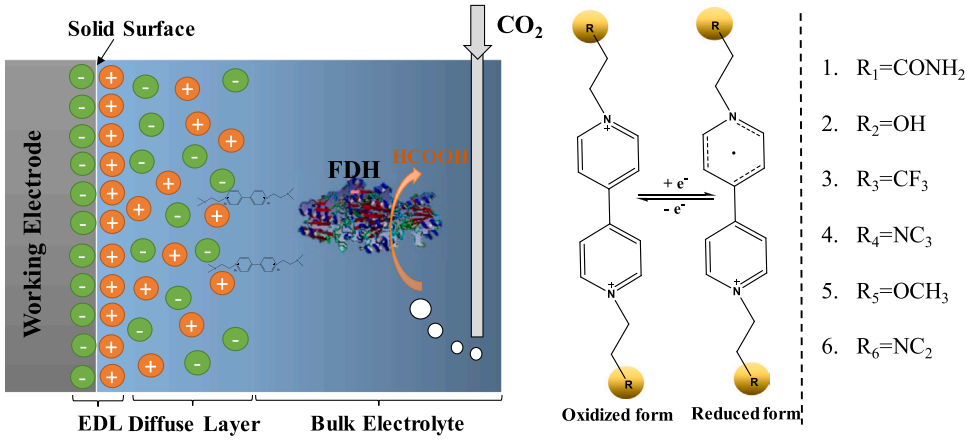

Fig. 1. (Left) Electroenzymatic conversion of CO_2 to formic acid, and (Right) chemical structures of the studied bipyridinium-based redox cofactors.

formic acid production, which can achieve a high selectivity by the enzymatic reaction and a low cost by electrocatalytic regeneration of cofactor. For example, Chen et al. [8] carried out electroenzymatic conversion of CO_2 to formic acid by coupling electrocatalytic regeneration of NADH with enzymatic CO_2 conversion, which sustainably achieves formic acid production at a low cost. Similarly, Zhang et al. [9] encapsulated enzymes in metal-organic framework coupling with electrocatalytic regeneration of NADH for CO_2 conversion. However, when NADH served as a cofactor, it suffered from instability and low efficiency for CO_2 conversion. Electrocatalytic reduction of NAD^+ to NADH is usually accompanied by the generation of byproducts, such as the dimer NAD_2 or isomer 1,6-NADH, which are inactive to formate dehydrogenase (FDH) and thus result in a permanent loss of cofactor [10]. Moreover, the enzymatic conversion of CO_2 to formic acid is reversible with an extremely low conversion when NADH serves as a cofactor, since the oxidation rate of formic acid to CO_2 is much faster than that of CO_2 reduction [7]. Therefore, improving the formic acid production efficiency and increasing the electro-recycling stability of the used cofactor still remain major challenges in practical applications.

Developing artificial cofactors to substitute the natural cofactor NADH is a novel and feasible way to address the above issues. Of which the artificial cofactors of bipyridinium-based salts (BP^{2+}) are particularly desirable candidates, which are able to receive electrons provided by a strong reductant or electrocatalytic reduction and simultaneously release electrons to FDH to achieve CO_2 enzymatic conversion. Importantly, BP^{2+} rarely drives the oxidation of formic acid back to CO_2, resulting in high efficiency of CO_2 reduction. Therefore, using artificial cofactors as electron carriers is a promising alternative to NADH and has the potential to substantially improve formic acid production. Indeed, it has been demonstrated that the production rate of formic acid was more than 20 times higher than that of NADH, by using the reduced 1,1′-dimethyl-4,4′-bipyridinium (methyl viologen, $MV^{+\bullet}$) [11]. Jayathilake et al. [12] reported a continuous electro-enzymatic conversion of CO_2 to formate by FDH with an electrochemical regeneration of $MV^{+\bullet}$ (methyl group), and the formate yield was found high up to 97% ± 1% over 30 h. In our group, Zhang et al. [13] tested the bipyridinium-based salts of 1,1′-dimethyl-4,4′-bipyridinium chloride (MV^{2+}), 1,1′-dicarboxymethyl-4,4′-bipyridinium bromine (DC^{2+}), and 1,1′-diaminoethyl-4,4′-bipyridinium bromine (DA^{2+}) as artificial cofactors for CO_2 enzymatic conversion. As a result, the formic acid concentration for the system with DA^{2+} was about 35 times higher than that of natural cofactor NADH. It is because that these functional groups in the pyridine ring could affect the electron transfer ability to substrates, and the amino group with stronger electron-donating and highest affinity for CO_2 presented the higher catalytic performance.

However, investigations of bipyridinium-based artificial cofactors are still scarce, and only the substitution groups in the pyridine ring, i.e., methyl, carboxylic and amino group, have been studied. Furthermore, it is still unclear how the ionic properties of artificial cofactor affect the electron transfer and thus the efficiencies of cofactor electrochemical regeneration and electroenzymatic conversion of CO_2. Based on our previous investigation, the artificial cofactors with a stronger electron-donating ability and substrate affinity were expected to achieve better catalytic performance. Therefore, in this study, a series of bipyridinium-based functional groups were formulated for the first time to explore the role of the functional groups in the catalytic mechanism, and to screen the most optimal artificial cofactor for potential practical applications. The specifically studied bipyridinium-based artificial cofactors contain the functional groups of amide, hydroxyl, carbon trifluoride, quaternary ammonium, methyl ether, and dimethylamine, respectively, and were designed and synthesized as shown in Fig. 1. The enzymatic conversion and electrocatalytic regeneration of cofactors were integrated for a sustainable and efficient formic acid production at a low cost. The cofactor electrochemical regeneration and catalytic performance in the enzymatic reaction were systematically studied. Furthermore, the thermodynamic properties, electrochemical properties of cofactors, and catalytic mechanism were investigated and discussed based on the experimental measurements, Molecular Dynamic (MD) simulations using the Umbrella sampling, and electronic structure calculations using Density Functional Theory (DFT) based methods, giving a deep insight into the effect of the functional groups in $BP^{2+}/BP^{+\bullet}$ on the reduction of CO_2 to formic acid.

2. Experimental section

2.1. Materials

Formate dehydrogenase (EC 1.2.1.2, homo-dimer, 76 kDa) from *Candida boidinii* (FDH), β-nicotinamide adenine dinucleotide in reduced and oxidized forms (NADH and NAD^+, >97 wt%), 4,4′-bipyridine, (2-bromoethyl)trimethylammonium bromide, 2-bromoethyl methyl ether, 2-chloro-N,N-dimethylethylamine hydrochloride, 2-bromoacetamide, 2-bromoethanol, 1,1,1-trifluoro-3-iodopropane, and acetonitrile were purchased from Sigma-Aldrich. CO_2 was purchased from AGA A/S (Sweden) with purity (>99.5%).

2.2. Synthesis of bipyridinium-based salts

The bipyridinium-based salts were separately synthesized according to the literature [14]. Briefly, 1,1′-dimethylethylamine-4,4′-bipyridinium chloride ($BPNC_2$) was synthesized by heating 4,4′-bipyridine at reflux with 2 times molar equivalent of chloro-N,N-dimethylethylamine hydrochloride in acetonitrile (200 mL) at 90 °C for 24 h. After the reaction, the solvent was removed by a rotary evaporator, and the residue

was dried under vacuum overnight at 50 °C. Likewise, other bipyridinium-based salts were synthesized following the same procedure. The structures of the bipyridinium-based salts were identified by ^{1}H NMR in the supporting information, confirming the successful synthesis.

2.3. Cyclic voltammetry measurements

The cyclic voltammogram of the bipyridinium-based salts was measured by using a typical H-type electrochemical cell separated by a Nafion 117 membrane (geometrical area: 2.27 cm^2) with a three-electrode system. A carbon cloth (1 ×1 cm^2), an Ag/AgCl electrode (2 M KCl solution), and a platinum electrode were used as the working, reference, and counter electrodes, respectively. The working and reference electrodes were placed in the cathode chamber (10 mL) with a 100 mM phosphate buffer (pH 7.0), and the counter electrode was placed in the anode chamber (10 mL) with a 100 mM H_2SO_4 solution as the electrolyte.

2.4. CO_2 reduction to formic acid with FDH and cofactors

The electrocatalytic reduction of CO_2 to formic acid was performed in a typical H-type electrochemical cell. 1 mM cofactor and 0.1 mg/mL FDH (5 U/mg) in 100 mM phosphate buffer (pH 7.0) were prepared and put in the cathode chamber. The electrolyte in the cathode chamber was pre-bubbled with CO_2 (30 mL/min) for 30 min to achieve a CO_2-saturated solution before starting the experiment, and the reaction was then initiated by applying a potential.

2.5. Analytical methods

The product formate concentrations were determined by the UV-Vis spectrophotometer according to the literature [15]. Specifically, solution A was prepared by dissolving 0.5 g citric acid and 10 g acetamide in 100 mL isopropanol, while solution B was prepared by dissolving 30 g sodium acetate in 100 mL water. The samples (100 μL) were then mixed with 0.2 mL of solution A, 10 μL solution B and 0.7 mL 100% acetic anhydride, and incubated at 50 °C for 2 h with occasional mixing. Yellow color in solution was generated and measured photometrically at 515 nm.

2.6. MD simulations

Assuming that the exceptional rate of CO_2 conversion when utilizing the $BPNC_2$ cofactor could be related to the affinity of the cofactor to the CO_2 molecule, we compared these affinities by calculating the changes of the Potential of Mean Force (PMF) when pulling the CO_2 molecule from outside of the FDH protein to inside. The path of CO_2 was chosen to pass along the molecular axis of the cofactors. To reduce the already high computational cost, we performed MD simulations only for the best and worst-performing cofactors identified from the experiments. The parametrization, the simulation protocols and conditions were the same as in our previous work [13]. To facilitate the comparison of the results, the X-ray structure of the FDH protein was downloaded from the protein data bank (PDB ID: 5DN9) [16], and all the other molecules were built using the Avogadro software [17]. The geometry of the cofactors was optimized using the GAUSSIAN software [18], and atomic point charges for the force field were calculated using an electrostatic potential (ESP) fit [19]. The ff19SB AMBER force field [20] was used to parametrize the protein, while the GAFF2 forcefield [21] was used for the cofactor and CO_2 molecule. H_3O^+ was simulated using the parameters developed by Baaden et al. [22], the ionsjc_tip3p was used for ions [23], and the TIP3P model [24] was used for water.

All-atom MD simulations were performed for both cofactors using the GROMACS 20.4 software [25] and the protocol described below. The simulation box was cubic with periodic boundary conditions (PBC), and the equations of motion of the atoms were integrated with a timestep of 2 fs. The cutoff radius for Van der Waals interactions was set to 12 Å, and the Particle Mesh Ewald (PME) [26] method was used to calculate the electrostatic interactions using a grid spacing of 1 Å. At each time step of 2 fs, we calculated the full electrostatic and non-bonded forces. The simulations were performed using the NpT ensemble, which implies utilizing the Parrinello-Rahman barostat for pressure control with the pressure value set at 1 bar and the v-rescale thermostat for temperature control with the temperature set to 297 K. LINCS algorithm [27] was used to constraint the length of bond of the hydrogen atom to their equilibrium lengths. Prior to the production runs, energy minimization, followed by equilibration runs, was performed to stabilize the system using constraints as described in our previous work [13]. In the production run, the pulling of the CO_2 molecule was achieved using the Umbrella pulling method over 40 windows with a pulling rate of 1 Å per window. In order to simplify the simulation, although the protein has a mirror structure with 2 active sites, only one natural cofactor was replaced with the artificial one. The evolution of the free energy of the system related to the position of the CO_2 molecule was calculated by employing the use of the Weighted Histogram Analysis Method (WHAM) [28].

2.7. Electronic structure calculations

The structure of all the studied cofactors, both in the reduced and oxidized form, was optimized by means of quantum mechanical calculations based on the density functional theory (DFT). The employed level of theory was UB3LYP/6–311 +g(d,p), as implemented in the suite of programs Gaussian 16 [18]. and the nature of the stationary states was confirmed as minima by vibrational analysis performed at the same level of theory. The reduced and the oxidized forms of each cofactor were optimized both in vacuo, and using a polarizable continuum model (PCM) for the water solvent within the integral equation formalism IEF-PCM [29] as implemented in Gaussian 16. Details on the geometry optimization are reported in the supporting information, and Tables S2–S5 summarize the relevant structural information concerning the optimized structure. Atomic dipole moment corrected Hirshfeld population (ADCH) charges [30] were calculated using the software Multiwfn [31].

The Fukui function is extensively used to predict the reactive sites, and we calculated the condensed Fukui f_k^- function using the ADCH charges. Specifically, to predict on which sites of the reduced cofactor the electrophilic attack should occur, we calculated the condensed Fukui function f_k^- defined as

$$f_k^- = q_k(N) - \quad q_k(N-1)$$

where $q_k(N)$ is the charge at atomic center k calculated on the reduced form of the cofactor ($BP^{+\bullet}$), and $q_k(N-1)$ is the corresponding oxidized form (BP^{2+}), both calculated on the UB3LYP/6-311 +g(d,p) optimized geometry of the reduced form. The electrophilic attack is likely to occur on the atoms with larger f_k^-.

Te electron attachment enthalpy (EAE) is the energy required to attach an electron to a given chemical species, and it was calculated as the total enthalpy difference at 298.15 K, between the doubly positive cation (for $BPCF_3^{2+}$, $BPOH^{2+}$, $BPOCH_3^{2+}$, $BPCONH_2^{2+}$) or the quadruple positive species ($BPNC_3^{4+}$, $BPNC_2^{4+}$) and the radical obtained by the attachment of the electron to such species.

$$M^+ + e^- \rightarrow M^\bullet$$

with $M^\bullet$: $BPCF_3^{+\bullet}$, $BPOH^{+\bullet}$, $BPOCH_3^{+\bullet}$, $BPCONH_2^{+\bullet}$, $BPNC_2^{3+\bullet}$, $BPNC_3^{3+\bullet}$ and M^+: $BPCF_3^{2+}$, $BPOH^{2+}$, $BPOCH_3^{2+}$, $BPCONH_2^{2+}$, $BPNC_2^{4+}$, $BPNC_3^{4+}$

$$EAE = E(M^\bullet) - E(e^-) - E(M^+)$$

Considering that the contribution of the electron is constant, and that we are interested in trends rather than in absolute values when

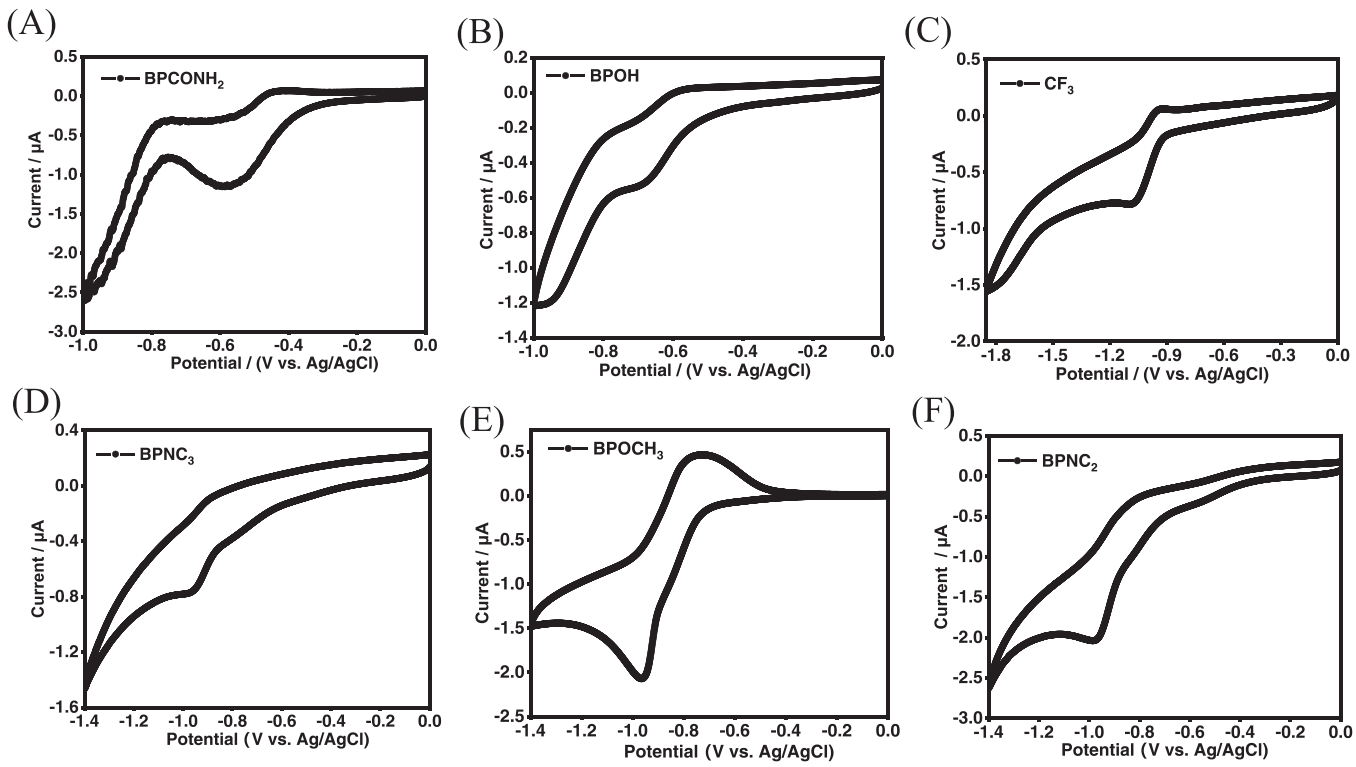

Fig. 2. CV curves of (A) $BPCONH_2$, (B) BPOH, (C) $BPCF_3$, (D) $BPNC_3$, (E) $BPOCH_3$ and (F) $BPNC_2$. Conditions: 1 mM cofactors in 100 mM phosphate buffer (pH 7.0) as electrolyte.

Table 1
Thermodynamic analysis.

Cofactors	E_{red}[a] (V vs SHE)[b]	ΔG (kJ/mol)	Equilibrium constant (K)	Ratio of K_x/K_{NAD}
NAD^+	-0.320	38.594	1.7×10^{-7}	1
$BPCONH_2$	-0.383	26.436	2.3×10^{-4}	1.3×10^{3}
BPOH	-0.493	5.2102	0.12	7.1×10^{5}
$BPCF_3$	-0.903	-73.907	8.9×10^{12}	5.2×10^{19}
$BPNC_3$	-0.763	-46.892	1.6×10^{8}	9.4×10^{14}
$BPOCH_3$	-0.763	-46.892	1.6×10^{8}	9.4×10^{14}
$BPNC_2$	-0.773	-48.821	3.6×10^{8}	2.1×10^{15}

[a] The reduction potential.
[b] $E_{SHE}=E_{Ag/AgCl}+E_{Ag/AgCl}$ vs NHE (0.197).

evaluating the performance of the co-factors, we have neglected the energy of the electron in the *EAE* calculations.

3. Results and discussion

3.1. Electrochemical properties of artificial cofactors

Electrochemical behavior of these artificial cofactors and natural cofactor NAD^+ was examined by using cyclic voltammetry (CV) in 100 mM phosphate buffer solution, where the carbon cloth, Pt wire, and Ag/AgCl were working electrode, counter electrode, and reference electrode, respectively. As shown in Fig. 2, the reduction peak in the CV curve represents the transformation from oxidized artificial cofactor to the reduced form, and likewise, the oxidation peak indicates the oxidation of reduced artificial cofactor to the oxidized form. The

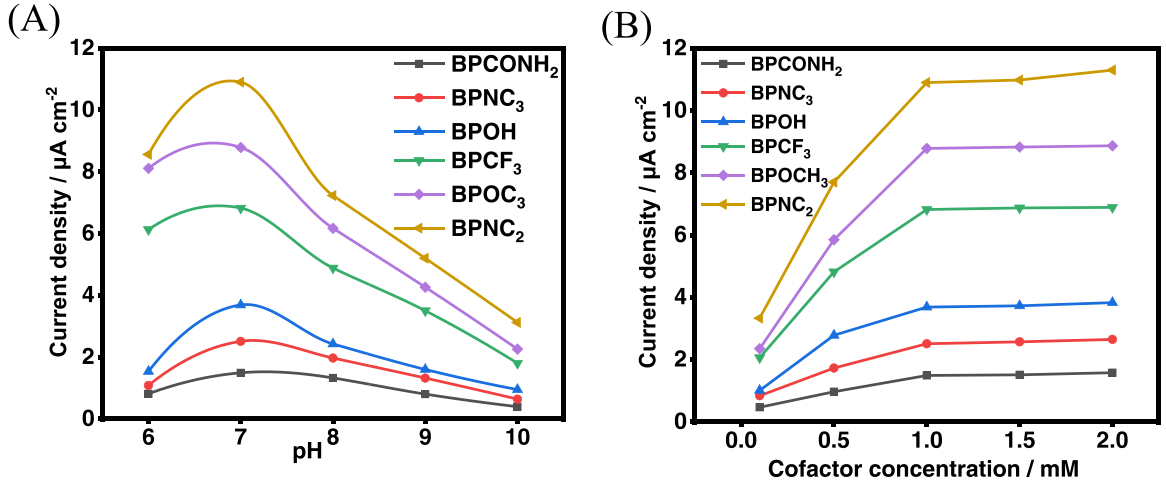

Fig. 3. Dependence of the electrocatalytic response on pH (A) and cofactor concentration (B).

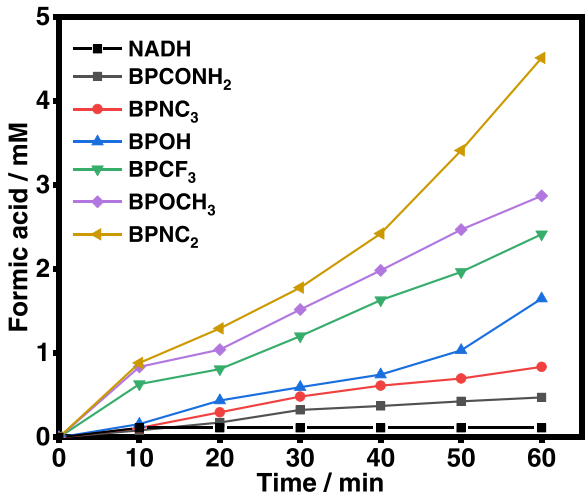

Fig. 4. The concentration of formic acid as a function of time with 1 mM different cofactors at their corresponding reduction peak potential vs. Ag/AgCl in 100 mM phosphate buffer (pH 7) as electrolyte.

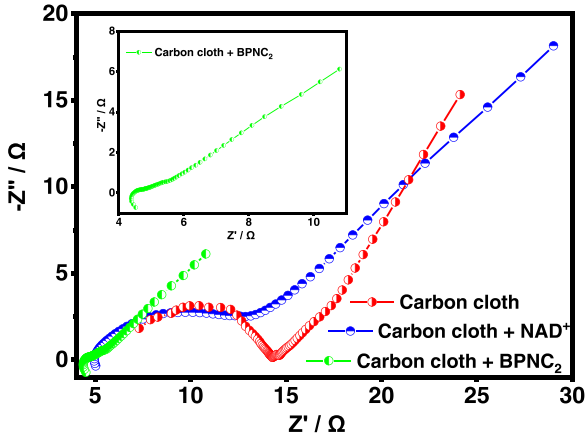

Fig. 5. Nyquist plots for a bare carbon cloth (CC) electrode, CC + NAD^+ (1 mM), CC + $BPNC_2$ (1 mM), in the presence of 5 mM $K_3Fe(CN)_6^{3-}$/ $K_4Fe(CN)_6$ in 0.1 M KCl solution. The electrode potential was based at 0.21 V (Versus Ag/AgCl).

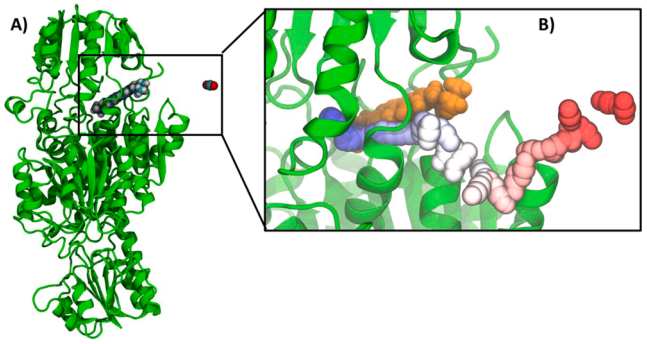

Fig. 6. A) Structure of the FDH protein highlighting the $BPNC_2$ cofactor that replaced the natural one and the initial position of the CO_2 molecule. B) Detailed representation of the position of the CO_2 molecule at the start of each Umbrella sampling window. The protein is represented as cartoon in green and the cofactor and the CO_2 molecule as VdW spheres. In detail B) the cofactor is colored in orange and the CO_2 molecule changes color from red at the beginning to white and to blue at the end.

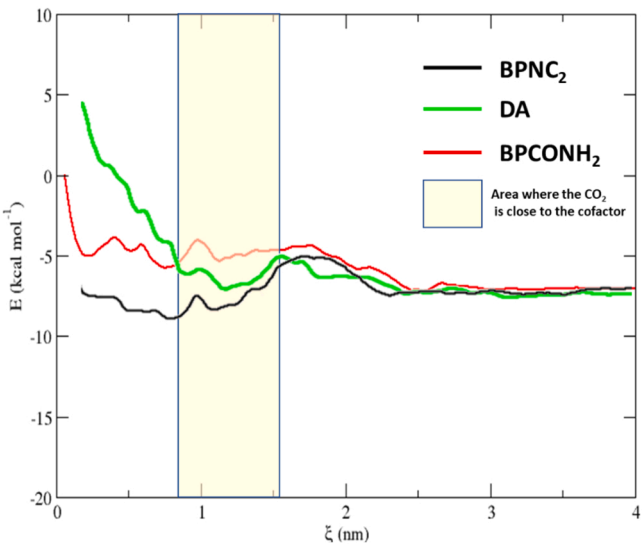

Fig. 7. Plots of the changes in free energy of the system with the movement of the CO_2 molecule from the outside (right) to the inside (left).

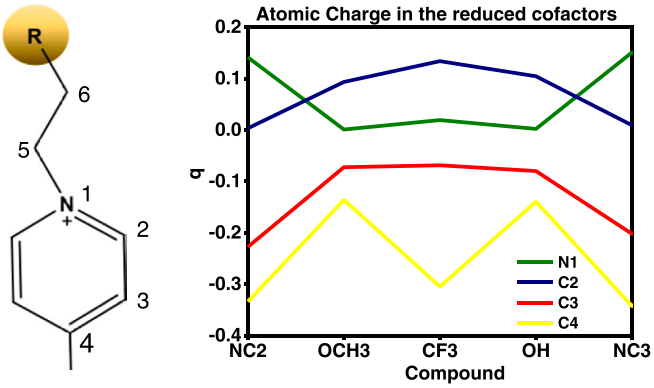

Fig. 8. (Left) Numbering of the heavy atoms in core part of BP. (Right) ADCH charges on the heavy atoms of the artificial cofactors core in the reduced form, averaged over chemically equivalent atoms.

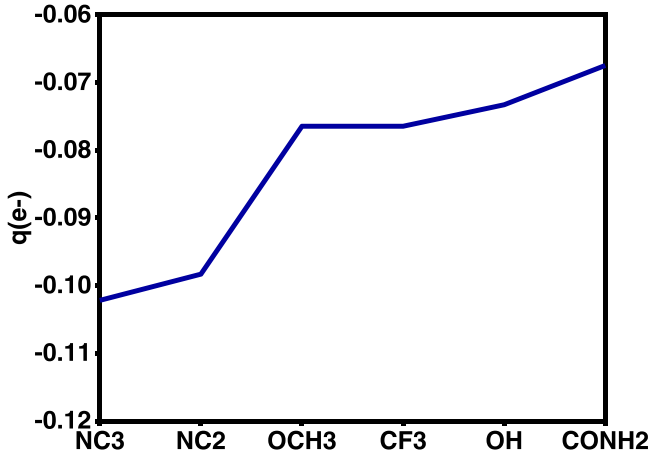

Fig. 9. Largest f_k^- values for each cofactor, considering the heavy atoms in the core moiety.

reduction potential of these artificial cofactors followed the order of $BPNC_2$ > $BPOCH_3$ > $BPCF_3$ > BPOH > $BPNC_3$ > $BPCONH_2$, indicating that the reduction potentials were affected by the functional group.

Table 2
EAE values calculated with IEFPCM solvent model for water.

	NC_2^{4+}	OCH_3^{2+}	CF_3^{2+}	OH^{2+}	NC_3^{4+}	$CONH_2^{2+}$
EAE (Hartree)	-0.168	-0.160	-0.166	-0.160	-0.169	-0.156

Moreover, the cyclic voltammogram of each artificial cofactor presents clearly reversible redox peaks, indicating that the reduced and oxidized forms could interconversion between each other driven by the electrochemical force, and thus all these artificial cofactors are recyclable for sustainably enzymatic conversion of CO_2.

For comparison, the natural cofactor NAD^+ presents an irreversible CV curve under the same conditions, indicating the oxidized and reduced natural cofactors could not be interconverted under the electrocatalysis when the carbon cloth was used as the cathode [13]. As a matter of fact, to achieve the electrocatalytic reduction of NAD^+ to NADH, noble metal-based electrodes (e.g., Rhodium) are generally needed, and subsequently, the electrode fabrication is complex, which usually hamper the large-scale application [9]. Moreover, under electrocatalysis, NAD^+ is easily reduced to dimer NAD_2 or isomer 1,6-NADH, both of which are inactive to FDH for enzymatic reaction and irreversible recovery, resulting in the permanent loss of this expensive cofactor [10]. Therefore, artificial cofactors are promising alternatives to the natural cofactor, owing to their low request for electrodes, recyclability under electrocatalysis, and their low cost compared to the natural cofactor.

3.2. Energy analysis

To elucidate the structure-energy relationship and catalytic performance of the artificial cofactors, thermodynamic parameters and equilibrium constants were estimated from the Nernst Equation. Among these artificial cofactors, the functional groups on bipyridine ring have great influences on ΔG and K. As shown in Table 1, the values of ΔG of artificial cofactors follow the order of $BPCONH_2$ > BPOH > $BPNC_3$ > $BPOCH_3$ > $BPNC_2$ > $BPCF_3$, and the lower value of ΔG indicates a more favorable thermodynamic driving force in the enzymatic conversion of CO_2 and thus higher yield of product. While, the equilibrium constant K follows the order of $BPCONH_2$ < BPOH < $BPNC_3$ < $BPOCH_3$ < $BPNC_2$ < $BPCF_3$, where a higher value of K indicates a higher yield of product, which is consistent with the results of ΔG. However, it has been stated that the strong nucleophilic ability of halogen elements on the functional group of CF_3 makes it easy to attack the protein, leading to a partial loss of cofactors that could not enter the active site of FDH. Indeed, according to the report [32,33], CF_3 can interact with the domain of nucleic acid-protein, resulting in partial loss of $BPCF_3$ as a cofactor in the reaction, and the rest can be served as the ligand for the enzyme. Therefore, the artificial cofactor with NC_2 could be the most efficient artificial cofactor.

In contrast, the enzymatic reaction with natural cofactor has a higher value of ΔG (38.59) and lower equilibrium constant K (1×10^{-7}) compared to the artificial cofactor, indicating natural cofactor has a lower thermodynamic driving force and lower conversion. Particularly, the equilibrium constant of the natural cofactor (1.7×10^{-7}) is 2×10^{15} times lower than the artificial cofactor $BPNC_2$ (3.6×10^{8}). Indeed, enzymatic conversion of CO_2 with the natural cofactor is less efficient, since the reaction is reversible and the oxidation rate of formic acid to CO_2 is much faster than the CO_2 reduction. Typically, to shift the equilibrium towards the formate generation, at least two orders of magnitude higher NADH concentration compared to the product formate concentration is needed, and the high cost of NADH deters the application of this solution [12]. Therefore, to improve the low conversion efficiency of the enzymatic reaction, using artificial cofactor with favorable thermodynamics and equilibrium constant presents a promising alternative and potentially high-efficient performance.

3.3. Dependence of the electrocatalytic response on the solution pH and cofactor concentration

Since the current density of a reaction could precisely reflect the reaction conversion as investigated above, it was used as an indicator for optimizing reaction conditions. First, the buffer solutions with a pH ranging from 6 to 10 were prepared for investigation and evaluation since pH plays a key role in reaction conversion by affecting enzyme activity and the ratio of substrates (CO_2/HCO_3^-). As shown in Fig. 3A, the maximum current density for each artificial cofactor follows the order of $BPCONH_2$ < $BPNC_3$ < BPOH < $BPCF_3$ < $BPOCH_3$ < $BPNC_2$, which is consistent with the results (order) of product concentration presented in Fig. 4, confirming again that electroenzymatic reaction can be reflected sensitively by the current intensity. The optimal pH for all artificial cofactors in the reaction is 7, which agrees with the optimal activity of FDH [7]. Besides, the molar ratio of substrates, i.e., CO_2, HCO_3^- and CO_3^{2-}, can be sensitively driven by pH, thus influencing CO_2 conversion. According to Bjerrum plot [34] illustrated in Fig. S2, after pH 7, HCO_3^- starts converting to CO_3^{2-} which cannot serve as the substrate for FDH. Thus, the concentration of substrates (CO_2 + HCO_3^-) decreases with further increasing pH, resulting in low conversion. Therefore, the optimal pH for the reaction is 7, which is reasonable as investigated.

On the other hand, cofactor concentration was evaluated as shown in Fig. 3B for the enzymatic reaction. Likewise, the maximum current density for each artificial cofactor follows the same order as that based on the pH evaluation. Moreover, the current density increased with the increase of the concentration of the cofactor up to 1 mM, and arrived at a relatively stable value afterwards, indicating 1 mM cofactor is an economic and efficient concentration for the reaction. Therefore, pH 7 and

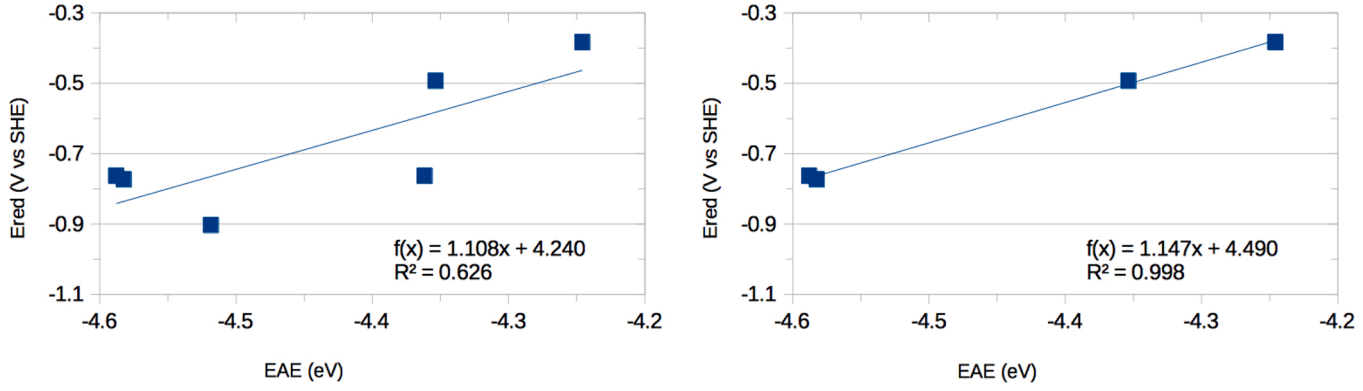

Fig. 10. Linear fitting of *EAE* values (calculated with IEFPCM solvent model for water) and the experimental reduction potentials of the six cofactors in water. The Pearson correlation coefficient is 0.791 taking into account all the compounds, and 0.999 excluding the data for the two compounds out of trend ($BPOCH_3^{2+}$, CF_3^{2+}).

1 mM cofactor give the optimized results.

3.4. Conversion of CO_2 to formic acid

To confirm an optimal cofactor for FDH, both the artificial cofactors and natural cofactor were tested in the enzymatic conversion of CO_2 to formic acid by applying their corresponding reduction peak potential vs. Ag/AgCl. As illustrated in Fig. 4, the concentrations of formic acid, at 60 min, were 0.47, 0.84, 1.6, 2.4, 2.9, 4.7, and 0.1 mM, for those with $BPCONH_2$, BPOH, $BPCF_3$, $BPNC_3$, $BPOCH_3$, $BPNC_2$, and NADH, respectively. As shown above, when using the natural cofactor, the formic acid concentration is much lower than those of artificial cofactors. It is because, when using the natural cofactor, the enzymatic reaction is reversible with an extremely low equilibrium constant. As a result, the formation of formic acid reached equilibrium quickly but with a very low concentration. Moreover, when using carbon cloth as the electrode, NAD^+ could not be reduced efficiently (around 1%) under electrocatalysis and thus cannot supply the reduced cofactor NADH for FDH, resulting in the low conversion of CO_2. The poor performance of NAD^+ reduction by carbon cloth electrode agreed with the observation of its CV [13], where the irreversible redox peaks confirmed the non-recyclability of NAD^+ by the carbon cloth electrode. Furthermore, the natural cofactor NADH cannot be stabilized in the weak acid, and would degrade to the unrecoverable isomers under pH 6.5, resulting in the permanent loss of active cofactor [35]. Also, CO_2 is a weak acid gas, which is unavoidable to participate in the reaction for CO_2 conversion and leads to the decrease of pH in the solution that will potentially degrade NADH. All in all, the natural cofactor is expensive, has poor stability, and is difficult to recycle, which impedes large-scale application.

While, compared to the natural cofactor, the artificial cofactors, with lower value ΔG and higher equilibrium constant K, present outstanding performance on the enzymatic conversion of CO_2. Particularly, the formic acid concentration for the system with $BPNC_2$ was 47 times higher than that of natural cofactor NADH at 60 min, indicating that the artificial cofactor $BPNC_2$ is stable, efficiently regenerated, and coupling enzymatic reaction for formic acid production. To further verify enzymatic reaction coupling with artificial cofactor $BPNC_2$ electroregeneration for formic acid production, the reaction was examined by chronoamperometry. As shown in Fig. S1, the enzymatic reaction with $BPNC_2$ was conducted in the absence of FDH, showing a lower current density (6.0 $\mu A/cm^2$). While, after the addition of FDH, the current density was enhanced to 14.9 $\mu A/cm^2$, indicating that enzymatic reaction coupling-reduced cofactor was conducted, and thus electron transfer was promoted.

During the electroenzymatic conversion of CO_2, cofactor $BPNC_2$ was reduced to radical $BPNC_2$ (reduced form) by applying the voltage for the reaction. While, the radical $BPNC_2$ itself is unstable, which can either be oxidized by the enzyme for CO_2 conversion or oxidized spontaneously by losing one electron in the aqueous solution, resulting in the generation of the oxidized $BPNC_2$. Therefore, interconversion between the oxidized and reduced $BPNC_2$ was carried out constantly once applying the voltage, indicating the artificial cofactor is recyclable and stable in the electroenzymatic reaction. For instance, 1 mM $BPNC_2$ in this study was initially added into the system and then 4.76 mM formic acid was generated, indicating 1 mM $BPNC_2$ was reduced more than 4 times recycles. Considering the loss of the oxidation of the radical $BPNC_2$ in the aqueous solution, much more $BPNC_2$ was reduced, indicating the desirable recycling and stability in the enzymatic reaction. To date, only few works have been reported to develop artificial cofactors for the electroenzymatic reduction of CO_2, which was summarized in our previous work [13]. Compare to the best results in the previous work (3.5 mM formic acid at 1 h), the yield of formate using $BPNC_2$ is higher (4.7 mM formic acid) under the same conditions. Therefore, the artificial cofactor $BPNC_2$ presents the best performance among all those studied, to our best knowledge.

3.5. Nyquist plots

The interface between electrode and electrolyte was investigated by the electrochemical impedance spectroscopy (EIS), for revealing the advantages of artificial ionic cofactor over the natural cofactors. As shown in Fig. 1, the interface was divided into three parts, i.e., electric double layer (EDL), diffusion layer, and bulk electrolyte. $K_3Fe(CN)_6$/$K_4Fe(CN)_6$ was used as a redox probe for the investigation, and the impedance changes for cofactor $BPNC_2$ and NAD^+ were separately conducted. Fig. 5 exhibits typical results of impedance spectra (Nyquist plots) of bare carbon cloth (CC), CC/NAD, and CC/$BPNC_2$. Here, Z′ and Z" are the real variable and the negatively imaginary variable of impedance, respectively. The figure showed a semi-circular part at high frequencies corresponding to the electron-transfer limited process (the electrode/solution interface) and a linear part at low frequencies to the diffusion process. R_{ct} has a little decrease (12.9 Ω) after the addition of NAD^+, indicating it has poor electron transfer ability and thus poor electro-reduction of NAD^+. While, by adding the artificial cofactor $BPNC_2$, the electron-transfer resistance decreased drastically and resulted in the lowest R_{ct} (5.2 Ω), indicating the cofactor accelerates the electron transfer probably, owing to the better conductivity of ionic cofactor compared to NAD^+. Thus, it results in the efficient reduction of artificial cofactors.

3.6. Molecular dynamics simulations

MD simulations were performed to evaluate the evolution of the free energy as the CO_2 molecule moves from the outside of the protein to the inside, and determine the affinity of the cofactors to the CO_2 molecule. We performed MD simulations only $BPNC_2$ with better efficiency than the previously reported cofactors (DA) [13] and the worst cofactor $BPCONH_2$. The simulations were realized using the exact same conditions as in our previous work, where we focused on a single reaction site in the FDH protein. Fig. 6 shows the starting structure of the protein with the $BPNC_2$ inserted inside and the CO_2 molecule outside and detailly depicting the initial position of the CO_2 molecule in each of the 40 windows.

Starting from the initial position of each window presented in Fig. 6B, we performed 402 ns umbrella sampling simulations. PMF was calculated using WHAM. The graphs are presented in Fig. 7. The plots represent the changes in free energy as the CO_2 molecule moves in each simulation. We have also added the plot for the DA cofactor that was previously reported in order to compare the results.

It can be seen that the changes in PMF of the systems are in accordance with the experimental observations, with the system having the lowest free energy in the region close to the $BPNC_2$ cofactor, the highest free energy in the region close to the $BPCONH_2$ cofactor, and the system with the DA cofactor situating itself between the other two. This points out that the $BPNC_2$ cofactor has the best affinity for the CO_2 molecule, which would explain the improved rate of CO_2 reduction. Also, it can be seen that for the $BPNC_2$ cofactor the free energy in its vicinity has a value lower than at the start of the simulation, where CO_2 is dissolved in water. This means that the reaction site has a better affinity towards the CO_2 molecule, increasing the probability that CO_2 enters the reaction site. This higher affinity could explain why the $BPNC_2$ cofactor has such a high reduction rate, as the CO_2 molecules would enter the reaction site more often and also remain for a longer period of time, which increase the probability of a productive positioning of the reactants for the product generation.

3.7. Analysis of the electronic structure of the artificial cofactors

To rationalize the different activities of the cofactors, we have verified by DFT calculations whether the nature of the R group can affect the electronic distribution on the BP moiety. The presence of two sp^3 carbon atoms between the R group and the BP region could reasonably prevent

any significant electronic effects. However, it is also possible that despite the presence of insulators between the substituents and aromatic groups, the electronic distribution on the latter can be affected [36].

The ADCH charges for the heavy atoms of the BP core are reported in Fig. 8 as averaged values over chemically equivalent atoms in the two symmetric moieties of BP.

It clearly can be seen from Fig. 8 (Right) that the variation of the R group has a large effect on the electronic distributions of the aromatic moiety. Indeed, the R group affects not only the partial charges of atom to which it is bound (C6), but also the farthest away atoms of the aromatic moiety, C3 and C4, and on all the atoms in between. Somehow counterintuitively, the substituents, NC_2 and NC_3, that have the largest positive charge, are those having the largest negative value in one of the atoms of the BP core; in detail, the C3 atom has a negative partial ADCH charge larger than 0.3. Similar consideration can be done also for the C2 atom, with the NC_2 and NC_3 groups leading to an increase of the negative charge on C2, while the effect of the other four substituents is similar. The charge on N atom in the aromatic moiety is positive with all R groups, with the positively charged NC_2 and NC_3 substituents leading to the smallest charge (close to zero), and the CO-NH_2 groups, to which correspond the least active compound, to the highest positive charge.

Analysis of the atomic charges gives an important insight into the capability of these substituents to modulate the electronic distribution on the BP core portion of the cofactor. However, it should be noticed that data in Fig. 8 indicates that the variation in the atomic charge does not correlate closely with the catalytic activity performance.

Fukui functions were used as a descriptor to understand the properties of catalysts for CO_2 reduction. Such descriptors have been recently successfully employed to rationalize the interaction of CO_2 with proteins [37], or the explain the performances of catalysts for CO_2 reduction of diverse nature [38,39]. We calculated the electrophilic condensed f function on the atoms of the cofactors (see numbering scheme in Fig. S3), as described in the section 2.7. In Fig. S4 are reported the f_k^- values calculated in vacuo on the heavy atoms of the core of the cofactor, averaged over equivalent atoms. In Fig. 9 are reported for each cofactor only the largest f_k^- values, and the atom on which they are located are indicated in Fig. S4. Larger negative values correspond to higher reactivity toward the electrophilic attack, which is of interest since the oxidation of the cofactor implies the loss of an electron.

The most reactive site in the cofactors can be either the C3 or the N1 atom, the latter being favored with OH and OCH_3 substituents (See Fig. S4). We note that, with the exception of compound NC_3, the values of f_k^- reported in Fig. 9 follow the order of the catalytic efficiency. However, this data should not be overemphasized, since to characterize the correlation between the f_k^- descriptor and the reactivity, an extended conformational analysis of the compounds in the active site, and a corresponding population averaged f_k^- calculation would be necessary [37]. Also the environmental effect on these descriptors, which is not trivial to include when the molecule is in a complex environment as a protein pocket, is expected to play a role in the electronic distribution of the molecules. Analysis of the solvent effect using an implicit solvent model for water (Fig. S5) leads to a similar conclusion to those drawn without solvent inclusion concerning the strong impact of the substituents on the electronic distribution, and on the most probable reactive sites, C3 and N1.

For several classes of compounds, the redox potential has been found to have a linear relationship with the electron affinity and the related properties of electron attachment energy, either neutral or more seldom charged [40,41]. We verified whether this relationship holds also for this class of compounds. Table 2 lists the EAE calculated on the six cofactors using a PCM solvent model for water, and in Fig. 10 the values are correlated with the reduction potential measured in water (see Table 1).

The Pearson correlation coefficient indicates a good correlation between the measured potential and the attachment enthalpies, and the agreement is excellent when excluding two of the compounds ($BPOCH_3^{2+}$, $BPCF_3^{2+}$). On the contrary, if the solvent is not taken into account, no correlation is observed, as shown in Fig. S6. While it is clear that inclusion of the implicit solvent is important for a proper calculation of the electron attachment energy, in agreement with what was observed before either for neutral or charged species [41,42], it is possible that for some compounds ($BPOCH_3^{2+}$, $BPCF_3^{2+}$) of the class studied here, even a more accurate treatment of the solvent might be necessary for obtaining a higher correlation with experimental values.

From the analysis of the electronic properties of the cofactors, we can conclude that despite the presence of two sp^3 carbon atoms between the substituent R and the heteroaromatic moiety, the substituent strongly impacts the electronic distribution in the latter, and that this effect can play a role in determining its reactivity and thus the catalytic efficiency.

4. Conclusions

In this study, six artificial cofactors were designed and synthesized for the enzymatic CO_2 reduction to formic acid. All the bipyridinium-based artificial cofactors presented a superior catalytic performance compared to the natural cofactor NADH, owing to the suppression of the reverse oxidation reaction. Specifically, the formic acid concentration by using the cofactor $BPNC_2$ is 47 times higher than that of NADH. In addition, the thermodynamic analysis indicates that artificial cofactors provide a stronger thermodynamic driving force in the reaction and present a higher equilibrium constant. Also, the electrochemical investigation demonstrated that the artificial ionic cofactor improves conductivity and thus enhances electron transfer and electrocatalytic regeneration of the cofactor. MD simulations give further molecular insight into the behavior of the cofactor, confirming $BPNC_2$ with the highest affinity of CO_2, which is consistent with the experimental observations. Last, ab initio calculations indicate that the functional groups R also affect the electronic distribution and the electron-donating capability of BP core, and interestingly the positively charged functional groups as NC_2 and NC_3 can surprisingly lead to an increased electron-donating capability of the heavy atoms belonging to the aromatic core, as revealed by the condensed Fukui f functions. The different catalytic activity of the artificial cofactors is therefore due to a combination of several contributions, comprising the affinity for CO_2, the effect on the electron-donating capability in the BP rings and also the reactivity of the functional group itself. Our analysis should pave the way to future systematic studies aimed at disentangling the relative weight of each contribution to find a quantitative structure-activity relationship.

CRediT authorship contribution statement

Zhibo Zhang: Methodology, Formal analysis, Visualization, Writing – original draft, Writing – review & editing. **Tudor Vasiliu:** Simulation Investigation, Writing – review & editing. **Fangfang Li:** Writing – review & editing. **Aatto Laaksonen:** Conceptualization, Writing – review & editing. **Xiangping Zhang:** Conceptualization, Writing – review & editing. **Francesca Mocci**: QM Investigation, Conceptualization, Writing – review & editing. **Xiaoyan Ji:** Conceptualization, Supervision, Writing – original draft, Writing – review & editing.

Declaration of Competing Interest

The authors declare that they have no known competing financial interests or personal relationships that could have appeared to influence the work reported in this paper.

Acknowledgments

Z. Zhang and X. Ji thank the financial support from the Kempe Foundation in Sweden. F. Li and X. Ji acknowledge the financial support

from the Swedish Energy Agency (P47500-1, P51239-1). A. Laaksonen acknowledges the Swedish Research Council for financial support, and partial support from the Ministry of Research and Innovation of Romania (CNCS – UEFISCDI, project number PN-III-P4-ID-PCCF-2016-0050, within PNCDI III). F. Mocci acknowledges financial support from Progetto Fondazione di Sardegna (Grant CUP: F72F20000230007) and Regione Autonoma della Sardegna (RASSR81788-2017).

Appendix A. Supporting information

Supplementary data associated with this article can be found in the online version at doi:10.1016/j.jcou.2022.101978.

References

[1] L. Jeffry, M.Y. Ong, S. Nomanbhay, M. Mofijur, M. Mubashir, P.L. Show, Greenhouse gases utilization: a review, Fuel 301 (2021), 121017.
[2] S.A. Al-Tamreh, M.H. Ibrahim, M.H. El-Naas, J. Vaes, D. Pant, A. Benamor, A. Amhamed, Electroreduction of carbon dioxide into formate: a comprehensive review, ChemElectroChem (2021) 3207–3220.
[3] G. Centi, E.A. Quadrelli, S. Perathoner, Catalysis for CO_2 conversion: a key technology for rapid introduction of renewable energy in the value chain of chemical industries, Energy Environ. Sci. 6 (6) (2013) 1711–1731.
[4] Z. Zhang, J. Tong, X. Meng, Y. Cai, S. Ma, F. Huo, J. Luo, B.-H. Xu, S. Zhang, M. Pinelo, Development of an ionic porphyrin-based platform as a biomimetic light-harvesting agent for high-performance photoenzymatic synthesis of methanol from CO_2, ACS Sustain Chem. Eng. (2021).
[5] K. Van Daele, B. De Mot, M. Pupo, N. Daems, D. Pant, R. Kortlever, T. Breugelmans, Sn-based electrocatalyst stability: a crucial piece to the puzzle for the electrochemical CO_2 reduction toward formic acid, ACS Energy Lett. 6 (12) (2021) 4317–4327.
[6] R. Kortlever, I. Peters, S. Koper, M.T.M. Koper, Electrochemical CO_2 reduction to formic acid at low overpotential and with high faradaic efficiency on carbon-supported bimetallic Pd-Pt nanoparticles, ACS Catal. 5 (7) (2015) 3916–3923.
[7] Z.B. Zhang, J. Muschiol, Y.H. Huang, S.B. Sigurdardottir, N. von Solms, A. E. Daugaard, J. Wei, J.Q. Luo, B.H. Xu, S.J. Zhang, M. Pinelo, Efficient ionic liquid-based platform for multi-enzymatic conversion of carbon dioxide to methanol, Green Chem. 20 (18) (2018) 4339–4348.
[8] Y.J. Chen, P. Li, H. Noh, C.W. Kung, C.T. Buru, X.J. Wang, X. Zhang, O.K. Farha, Stabilization of formate dehydrogenase in a metal-organic framework for bioelectrocatalytic reduction of CO_2, Angew. Chem. Int. Ed. 58 (23) (2019) 7682–7686.
[9] Z.B. Zhang, J.J. Li, M.B. Ji, Y.R. Liu, N. Wang, X.P. Zhang, S.J. Zhang, X.Y. Ji, Encapsulation of multiple enzymes in a metal-organic framework with enhanced electro-enzymatic reduction of CO_2 to methanol, Green Chem. 23 (6) (2021) 2362–2371.
[10] X.D. Wang, T. Saba, H.H.P. Yiu, R.F. Howe, J.A. Anderson, J.F. Shi, Cofactor NAD (P)H regeneration inspired by heterogeneous pathways, Chem 2 (5) (2017) 621–654.
[11] Y. Amao, S. Ikeyama, Discovery of the reduced form of methylviologen activating formate dehydrogenase in the catalytic conversion of carbon dioxide to formic acid, Chem. Lett. 44 (9) (2015) 1182–1184.
[12] B.S. Jayathilake, S. Bhattacharya, N. Vaidehi, S.R. Narayanan, Efficient and selective electrochemically driven enzyme-catalyzed reduction of carbon dioxide to formate using formate dehydrogenase and an artificial cofactor, Acc. Chem. Res. 52 (3) (2019) 676–685.
[13] Z. Zhang, T. Vasiliu, F. Li, A. Laaksonen, F. Mocci, X. Ji, Electrochemically driven efficient enzymatic conversion of CO_2 to formic acid with artificial cofactors, J. CO2 Util. 52 (2021), 101679.
[14] S. Ikeyama, Y. Amao, An artificial co-enzyme based on the viologen skeleton for highly efficient CO_2 reduction to formic acid with formate dehydrogenase, ChemCatChem 9 (5) (2017) 833–838.
[15] R.K. Singh, R. Singh, D. Sivakumar, S. Kondaveeti, T. Kim, J.L. Li, B.H. Sung, B. K. Cho, D.R. Kim, S.C. Kim, V.C. Kalia, Y.H.P.J. Zhang, H.M. Zhao, Y.C. Kang, J. K. Lee, Insights into cell-free conversion of CO_2 to chemicals by a multienzyme cascade reaction, ACS Catal. 8 (12) (2018) 11085–11093.
[16] Q. Guo, L. Gakhar, K. Wickersham, K. Francis, A. Vardi-Kilshtain, D.T. Major, C. M. Cheatum, A. Kohen, Structural and kinetic studies of formate dehydrogenase from Candida boidinii, Biochemistry 55 (19) (2016) 2760–2771.
[17] M.D. Hanwell, D.E. Curtis, D.C. Lonie, T. Vandermeersch, E. Zurek, G.R. Hutchison, Avogadro: an advanced semantic chemical editor, visualization, and analysis platform, J. Cheminform. 4 (2012).
[18] G.W.T.M.J. Frisch, H.B. Schlegel, G.E. Scuseria, M.A. Robb, J.R. Cheeseman, G. Scalmani, V. Barone, G.A. Petersson, H. Nakatsuji, X. Li, M. Caricato, A. Marenich, J. Bloino, B.G. Janesko, R. Gomperts, B. Mennucci, H.P. Hratchian, J.V. Ortiz, A.F. Izmaylov, J.L. Sonnenberg, D. Williams-Young, F. Ding, F. Lipparini, F. Egidi, J. Goings, B. Peng, A. Petrone, T. Henderson, D. Ranasinghe, V.G. Zakrzewski, J. Gao, N. Rega, G. Zheng, W. Liang, M. Hada, M. Ehara, K. Toyota, R. Fukuda, J. Hasegawa, M. Ishida, T. Nakajima, Y. Honda, O. Kitao, H. Nakai, T. Vreven, K. Throssell, J.A. Montgomery, Jr., J.E. Peralta, F. Ogliaro, M. Bearpark, J.J. Heyd, E. Brothers, K.N. Kudin, V.N. Staroverov, T. Keith, R. Kobayashi, J. Normand, K. Raghavachari, A. Rendell, J.C. Burant, S.S. Iyengar, J. Tomasi, M. Cossi, J.M. Millam, M. Klene, C. Adamo, R. Cammi, J.W. Ochterski, R.L. Martin, K. Morokuma, O. Farkas, J.B. Foresman, D.J. Fox, Gaussian 16 Rev. A.03, Wallingford, CT 2016.
[19] C.I. Bayly, P. Cieplak, W.D. Cornell, P.A. Kollman, A. Well-Behaved, Electrostatic potential based method using charge restraints for deriving atomic charges – the Resp model, J. Phys. Chem. 97 (40) (1993) 10269–10280.
[20] C. Tian, K. Kasavajhala, K.A.A. Belfon, L. Raguette, H. Huang, A.N. Migues, J. Bickel, Y.Z. Wang, J. Pincay, Q. Wu, C. Simmerling, ff19SB: amino-acid-specific protein backbone parameters trained against quantum mechanics energy surfaces in solution, J. Chem. Theory Comput. 16 (1) (2020) 528–552.
[21] J.M. Wang, R.M. Wolf, J.W. Caldwell, P.A. Kollman, D.A. Case, Development and testing of a general amber force field, J. Comput. Chem. 25 (9) (2004) 1157–1174.
[22] M. Baaden, M. Burgard, G. Wipff, TBP at the water-oil interface: the effect of TBP concentration and water acidity investigated by molecular dynamics simulations, J. Phys. Chem. B 105 (45) (2001) 11131–11141.
[23] I.S. Joung, T.E. Cheatham, Molecular dynamics simulations of the dynamic and energetic properties of alkali and halide ions using water-model-specific ion parameters, J. Phys. Chem. B 113 (40) (2009) 13279–13290.
[24] P. Mark, L. Nilsson, Structure and dynamics of the TIP3P, SPC, and SPC/E water models at 298 K, J. Phys. Chem. A 105 (43) (2001) 9954–9960.
[25] D. Van der Spoel, E. Lindahl, B. Hess, G. Groenhof, A.E. Mark, H.J.C. Berendsen, GROMACS: fast, flexible, and free, J. Comput. Chem. 26 (16) (2005) 1701–1718.
[26] U. Essmann, L. Perera, M.L. Berkowitz, T. Darden, H. Lee, L.G. Pedersen, A. Smooth, Particle mesh ewald method, J. Chem. Phys. 103 (19) (1995) 8577–8593.
[27] B. Hess, H. Bekker, H.J.C. Berendsen, J.G.E.M. Fraaije, LINCS: a linear constraint solver for molecular simulations, J. Comput. Chem. 18 (12) (1997) 1463–1472.
[28] S. Kumar, D. Bouzida, R.H. Swendsen, P.A. Kollman, J.M. Rosenberg, The weighted histogram analysis method for free-energy calculations on biomolecules. 1. The method, J. Comput. Chem. 13 (8) (1992) 1011–1021.
[29] G. Scalmani, M.J. Frisch, Continuous surface charge polarizable continuum models of solvation. I. General formalism, J. Chem. Phys. 132 (11) (2010).
[30] T. Lu, F.W. Chen, Atomic dipole moment corrected hirshfeld population method, J. Theor. Comput. Chem. 11 (1) (2012) 163–183.
[31] T. Lu, F.W. Chen, Multiwfn: a multifunctional wavefunction analyzer, J. Comput. Chem. 33 (5) (2012) 580–592.
[32] G.A. Korshunova, N.V. Sumbatyan, A.N. Topin, M.T. Mtchedlidze, Photoactivatable reagents based on aryl(trifluoromethyl) diazirines: synthesis and application for studying nucleic acid-protein interactions, Mol. Biol. 34 (6) (2000) 823–839.
[33] R. Rajan, P. Balaram, A model for the interaction of trifluoroethanol with peptides and proteins, Int. J. Pept. Prot. Res. 48 (4) (1996) 328–336.
[34] C.B. Andersen, Understanding carbonate equilibria by measuring alkalinity in experimental and natural systems, J. Geosci. Educ. 50 (2002), 357-36.
[35] Z.B. Zhang, B.H. Xu, J.Q. Luo, N. Von Solms, H.Y. He, Y.Q. Zhang, M. Pinelo, S. J. Zhang, Ionic liquids as bifunctional cosolvents enhanced CO_2 conversion catalysed by NADH-dependent formate dehydrogenase, Catalysts 8 (8) (2018).
[36] G. Cerioni, E. Maccioni, M.C. Cardia, S. Vigo, F. Mocci, Characterization of 2,5-diaryl-1,3,4-oxadiazolines by multinuclear magnetic resonance and density functional theory calculations. Investigation on a case of very remote Hammett correlation, Magn. Reson. Chem. 47 (9) (2009) 727–733.
[37] J. Oller, D.A. Saez, E. Vohringer-Martinez, Atom-condensed fukui function in condensed phases and biological systems and its application to enzymatic fixation of carbon dioxide, J. Phys. Chem. A 124 (5) (2020) 849–857.
[38] N. Melis, F. Mocci, A. Vacca, L. Pilia, Novel homogeneous selective electrocatalysts for CO_2 reduction: an electrochemical and computational study of cyclopentadienyl-phenylendiamino-cobalt complexes, Sustain. Energy Fuels 4 (11) (2020) 5609–5617.
[39] S. Gusarov, S.R. Stoyanov, S. Siahrostami, Development of Fukui function based descriptors for a machine learning study of CO_2 reduction, J. Phys. Chem. C 124 (18) (2020) 10079–10084.
[40] D.H. Evans, One-electron and two-electron transfers in electrochemistry and homogeneous solution reactions, Chem. Rev. 108 (7) (2008) 2113–2144.
[41] U. Azzena, M. Carraro, L. Pisano, F. Mocci, S. Antonello, F. Maran, Reducing properties of 1,2-dipyridyl-1,2-disodioethanes: chemical validation of theoretical and electrochemical predictions, RSC Adv. 6 (52) (2016) 46813–46821.
[42] A.P. Davis, A.J. Fry, Experimental and computed absolute redox potentials of polycyclic aromatic hydrocarbons are highly linearly correlated over a wide range of structures and potentials, J. Phys. Chem. A 114 (46) (2010) 12299–12304.